Journal of
MARINE RESEARCH

Volume 39, Number 1

On the dynamics of equatorial outflows with application to the Amazon's basin

by Doron Nof[1]

ABSTRACT

A simplified model is considered in order to describe the dynamics of outflows of rivers or sea straits located at or near the equator. The model is steady, frictionless and nondiffusive but the motions are not constrained to be quasigeostrophic. The geometry of the oceanic basin into which the outflow debouches is approximated by a wedge and the vertical structure of the flow is represented by two layers of different densities. Approximate solutions to the potential vorticity equation and the Bernoulli integral are obtained analytically.

It is found that, due to the β effect, an equatorial outflow is deflected toward or away from the coasts depending on the basin geometry and the direction of its axis. The deflection is accompanied by separation and "blocking" which results in coastal or equatorial trapping. When the angle between the coastlines forming the basin is larger than 120° and the basin's axis of symmetry is directed toward the northeast, as is the case of the Amazon's basin, the outflow is deflected away from the coasts and separates from both walls. Consequently, the outflow penetrates into the ocean interior as an isolated current.

A possible application of this theory to the processes responsible for the formation of isolated lenses containing Amazonian water, such as those observed off the South American Coast, is discussed. It is shown that these isolated lenses may be related to the profound seasonal variability of the Amazon's discharge and the subsequent variability of the separation points. Such a variability can lead to a seasonal formation of isolated segments containing Amazonian water which undergo geostrophic adjustment, close upon themselves, and form isolated lenses.

1. Cooperative Institute for Marine and Atmospheric Studies (CIMAS) and the Division of Meteorology and Physical Oceanography, Rosenstiel School of Marine and Atmospheric Science, 4600 Rickenbacker Causeway, Miami, Florida, 33149, U.S.A.

1. Introduction

The Amazon outflow represents a unique problem because of the geographical location of the mouth (at the equator) and the immense fresh water discharge [~200,000 m^3/sec (Davis, 1964; Gibbs, 1970)]. The Amazon fresh water discharge is so great that in terms of its effect on the salinity budget of the ocean, the Amazon supplies a "salinity anomaly" (the discharge times the salinity difference between the ocean and the source) which is twice as large as the one supplied by the Mediterranean outflow. Furthermore, the water of the Amazon maintains its identity as a stream penetrating far into the Atlantic Ocean.

During the last two decades interesting features related to this penetration have been observed. Ryther *et al.* (1967) and Gibbs (1970) have documented the presence of isolated low salinity lenses off the South American Coast, Froelich *et al.* (1978) observed similar lenses as far as the Caribbean Sea, and Landis (1971) described low salinity pockets east of Barbados. These low salinity lenses usually have a diameter of several hundred kilometers and a depth of ~20-40m; an example of such a lens is shown in Figure 1. Since the presence of a thin fresh water layer in the upper ocean affects the structure of the mixed layer, it is reasonable to expect that such relatively large low density lenses will affect the interaction of the ocean and the atmosphere and might also influence the local climate.

Because of these features, it is of interest to investigate the nature of the Amazon-Ocean interaction. To do this we simplify the problem to that of a channel emptying into an otherwise undisturbed equatorial ocean. As the river water spreads in the open ocean it experiences changes in the local planetary vorticity which must be offset by local changes in the structure of the flow. Our aim is to study the general characteristics of this process and to examine the mechanisms which may lead to a formation of isolated lenses. We do not intend to simulate the details of the real system; we merely hope to preserve enough analogy to the real system so that our results will give insight into natural phenomena.

There have been a number of previous investigations of rivers outflows dynamics (e.g., Takano, 1954, 1955; Paul and Lick, 1974; Nof, 1978a, b) but none of these investigations examined the influence of a variable Coriolis parameter which plays a major role in the problem under consideration. To simplify the analysis we shall consider a two-layer inviscid nondiffusive model whose motions are driven solely by the river discharge (Fig. 2). In other words, the effects of wind and longshore currents, such as the Guiana Current, are not taken into account so that the basin would have been stagnant had the Amazon not been flowing into it.

In contrast to most rivers, the Amazon estuary does not have a salt wedge apparently due to its relatively shallow depth at the mouth (~12m) and its large discharge (Gibbs, 1970). Therefore, we adopt a model which contains two sections; the flow in the feeding channel consists of one layer while the basin consists of two

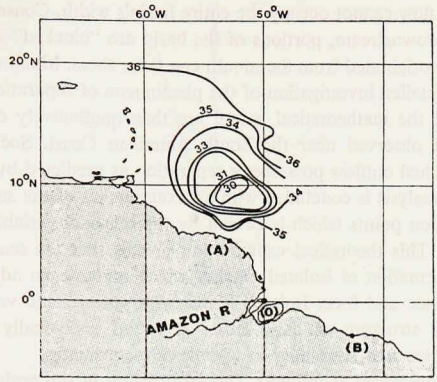

Figure 1. The Amazon's basin and the observed salinity structure of a typical low-salinity lens (adapted from Ryther *et al.*, 1967). Salinity concentrations are given in parts per thousand (‰). The lowest salinity is in the lens' core and equals ~24‰.

layers (Fig. 2). The lower layer is assumed to be very deep and its velocity (but not necessarily the transport) is neglected.

The geometry of the model has been chosen in such a way as to simplify the boundary conditions and to ensure that the problem is well posed. The hydrostatic assumption is invoked, but the motions are not constrained to be quasigeostrophic in the sense that the Rossby number characterizing the flow is not necessarily small. The flow is governed by two nonlinear equations, the potential vorticity and the Bernoulli equation. By using a power series expansion in $\epsilon = b/l$, the ratio of the width of the estuary to the length scale of the flow in the open ocean, the potential vorticity equation is reduced to a second-order partial differential equation. This equation indicates that as the flow spreads in the basin and advances into the open ocean, the relative vorticity ($\xi = \partial v/\partial x - \partial u/\partial y$) must decrease in order to compensate for the increase in planetary vorticity. With the aid of the same power series expansion, the Bernoulli integral is reduced to an algebraic equation relating the upper layer depth to the upstream depth. This relationship indicates that to zeroth-order the depth of the upper layer in the basin is uniform and does not vary with x or y.

The reduced potential vorticity equation and the zeroth-order Bernoulli integral are then combined to a single linear second-order partial differential equation of the elliptic type, the so-called Poisson equation. Its solution is found by elementary methods and by means of third order polynomials. It shows that when the fluid reaches a "critical" distance from the mouth its relative negative vorticity becomes

so large that the flow cannot occupy the entire basin's width. Consequently, separation occurs and downstream, portions of the basin are "blocked" in the sense that no parcels which originated from the mouth can enter them. Much of the discussion is devoted to a detailed investigation of the phenomena of separation and blocking.

The results of the mathematical model are then qualitatively compared to the salinity structure observed near the South American Coast. Such a comparison shows that the actual outflow possesses a separation as predicted by the mathematical model. The analysis is concluded with an examination of the seasonal variability of the separation points which is caused by the seasonal variability of the fresh water discharge. This theoretical examination reveals that the seasonal variability may lead to a formation of isolated patches which undergo an adjustment toward geostrophic balance and form isolated lenses with anticyclonic vorticity. The detailed theoretical structure of these lenses is found analytically by solving the equations of motion and continuity in cylindrical coordinates.

This paper is organized as follows: The formulation of the problem is discussed in Section 2. Section 3 contains the general mathematical analysis and Section 4 includes the zeroth-order solution. Sections 5 and 6 examine eastward and northward outflows, and the applicability of the model to the Amazon's basin is discussed in Section 7. Section 8 examines the processes which may lead to isolated lenses and Section 9 summarizes this work.

2. Formulation

We consider a two-layer model as shown in Figure 2. As mentioned earlier, the flow in the feeding channel consists of one layer since the Amazon's estuary does not contain a salt wedge. The lower layer in the basin is taken to be deep and its velocity (but not necessarily the transport) is neglected. We shall focus our attention on the region up to a distance of $\sim$ 500 km from the mouth. In this domain the coastline can be approximately represented by two straight lines as can be seen from Figure 1. The northern portion of the coast is directed approximately toward the NNW and the southern toward the ESE. The x axis is chosen such that it divides the basin into two equal parts and its direction coincides with that of the flow at the mouth. Under such conditions, the y axis is not directed toward the north but rather toward $(360° - \alpha_2)$ as shown in Figure 2. This choice of coordinates system slightly complicates the representation of the Coriolis parameter but because of the basin's geometry it simplifies considerably the mathematical analysis and is the most convenient coordinates system for the problem.

The flow in the active layer is taken to be steady, inviscid and nondiffusive, and the pressure is assumed to be hydrostatic. The effect of the earth's rotation is represented by the familiar equatorial β-plane approximation. For hydrostatic motions the horizontal pressure gradients depend on x and y alone; therefore, the horizontal

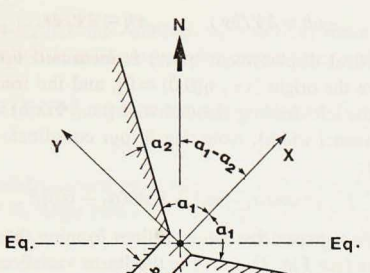

TOP VIEW

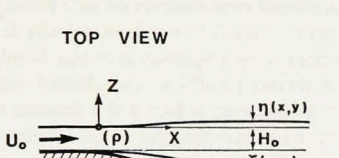

SIDE VIEW

Figure 2. Schematic diagram of the model under study. The straight lines forming the basin into which the outflow debouches represent sections OA and OB of the actual coastline (see Fig. 1). The free surface displacement η is measured upward from the free surface above the origin [i.e. $\eta(0,0) = 0$]. The interface displacement ζ is measured downward from the channel depth at $x = y = 0$. H_o is the river depth at the mouth.

velocity components (u,v) are taken to be independent of depth. For such conditions the potential vorticity equation and the Bernoulli integral are (see e.g., Gutman, 1972):

$$\nabla_H \cdot (\nabla_H \Psi/h) + f = hK(\Psi) \tag{2.1}$$

and

$$\tfrac{1}{2}(\nabla_H \Psi/h)^2 + g\eta = G(\Psi) \ , \tag{2.2}$$

where $K(\Psi) = dG(\Psi)/d\Psi$, ∇_H is the horizontal del-operator, f the Coriolis parameter, h the total depth of the fluid column, g the acceleration of gravity, η the free surface displacement and Ψ a transport function defined by:

$$-uh = \partial\Psi/\partial y\,; \qquad vh = \partial\Psi/\partial x. \tag{2.3}$$

The free surface vertical displacement $\eta(x,y)$ is measured upward from the free surface directly above the origin [i.e., $\eta(0,0) = 0$], and the transport function Ψ is taken to be zero at the left[2] feeding channel wall [i.e., $\Psi(x,b) = 0$; $x \leqslant 0$, where b is half the feeding channel width]. Note that in our coordinate system the Coriolis parameter is given by:

$$f = [x\cos(\alpha_1 - \alpha_2) + y\sin(\alpha_1 - \alpha_2)]\beta\,, \tag{2.4}$$

where $2\alpha_1$ is the angle between the two coastlines forming the basin, α_2 the tilt of the northern coastline (see Fig. 2) and β is the linear variation of the Coriolis parameter with latitude.

The functions $K(\Psi)$ and $G(\Psi)$ are to be determined from the conditions at the outlet to the basin which must be specified. Following Takano (1954, 1955) and Nof (1978a, b) who considered river outflows on an f plane, we assume that when the river enters the ocean ($-b \leqslant y \leqslant b$; $x = 0$) its velocity is unidirectional ($v = 0$) and does not vary in a cross-stream direction ($u = U_0$). In other words, it is assumed that the streamlines remain parallel to the channel walls until the outlet is reached; in reality some modification is expected a distance of $0(b)$ upstream from the outlet. It will become clear later that this approximation has a minor effect on the field although the initial details of the flow in the basin will be altered a distance of $0(b)$ from the mouth.

3. Analysis

a. Governing equations. We shall first evaluate the functions $K(\Psi)$ and $G(\Psi)$ from the conditions at the outlet to the basin. Since the flow at the outlet to the basin ($-b \leqslant y \leqslant b$; $x = 0$) is taken to be unidirectional ($v = 0$) it follows from the y component of the momentum equation $[u(\partial v/\partial x) + v(\partial v/\partial y) + fu = -g(\partial\eta/\partial y]$ that the horizontal pressure gradient across the feeding channel is balanced by the Coriolis force [i.e., $fu = -g(\partial\eta/\partial y)$]. In view of this and (2.4), the free surface vertical displacement at the outlet ($x = 0$) is:

$$\eta_u = -\beta U_0 y^2 \sin(\alpha_1 - \alpha_2)/2g, \tag{3.1}$$

where the subscript "u" indicates that the variable in question is associated with the upstream conditions.

To simplify the upstream conditions we shall further assume that at the outlet the channel bottom is not flat but rather has a transversal slope of $dZ_B/dy = d\eta_u/dy$, where Z_B is the bottom elevation. With such conditions the column depth H_o at the outlet is independent of cross-stream direction y. It will become clear later that this assumption of a particular bottom slope at the outlet can be avoided because $\eta_u(y)$

2. Hereafter, left and right are with reference to an observer looking downstream.

is much smaller than H_o [for the Amazon, $\eta_u \sim 0(1\text{cm})$ while $H_o \sim 0(10\text{m})$]. That is to say, the assumption is made merely for convenience and is not essential for the general analysis.

Application of the assumed conditions at the mouth ($u = U_o$; $v = 0$) to (2.1) gives:

$$K(\Psi) = f(\Psi)/H_o\,,$$

where $f(\Psi)$ is the Coriolis parameter at the outlet ($-b \leqslant y \leqslant b$; $x = 0$) expressed as a function of Ψ, and H_o is the uniform outlet depth. With the aid of (2.4) one finds that $K(\Psi) = [\beta y(\Psi)\sin(\alpha_1 - \alpha_2)]/H_o$, which by considering the relationship between Ψ and y at the outlet [$\Psi = -U_oH_o(y - b)$] gives:

$$K(\Psi) = \frac{\beta}{H_o}\,(b - \Psi/U_oH_o)\,\sin(\alpha_1 - \alpha_2). \tag{3.2}$$

Similarly, the function $G(\Psi)$ is found, from the conditions at the outlet and (2.2) to be:

$$G(\Psi) = \tfrac{1}{2}U_o^2 - \frac{\beta U_o}{2}\,(b - \Psi/U_oH_o)^2\sin(\alpha_1 - \alpha_2), \tag{3.3}$$

which satisfies the condition $dG(\Psi)/d\Psi = K(\Psi)$ as required.

In order to determine the general structure of the governing equations, it is necessary to find the relationship between the free surface vertical displacement η and the total depth of the upper layer in the basin (h). Since there is no pressure gradient in the lower layer, the free surface vertical displacement is given by:

$$\eta \approx \frac{\Delta\rho}{\rho}\,\zeta\,, \tag{3.4}$$

where ρ is the density of the upper layer, $\Delta\rho$ ($<< \rho$) the density difference between the layers and ζ is the interface vertical displacement [measured downward from the origin (i.e., $\zeta(0,0) = 0$)]. Hence, $|\eta| << |\zeta|$ and h ($= H_o + \eta + \zeta$) can be approximated by ($H_o + \zeta$) so that (3.4) takes the approximate form:

$$\eta = \frac{\Delta\rho}{\rho}\,(h\text{-}H_o). \tag{3.5}$$

The general form of the governing equations is now found by inserting (3.2), (3.3) and (3.5) into (2.1) and (2.2):

$$\nabla_H \cdot (\nabla_H\Psi/h) + \beta[x\cos(\alpha_1 - \alpha_2) + y\sin(\alpha_1 - \alpha_2)]$$
$$= \frac{\beta h}{H_o}\,(b - \Psi/U_oH_o)\,\sin(\alpha_1 - \alpha_2) \tag{3.6}$$

$$\tfrac{1}{2}(\nabla_H\Psi/h)^2 + g'(h - H_o) = \frac{U_o^2}{2} + \frac{\beta U_o}{2}\,(b - \Psi/U_oH_o)^2\sin(\alpha_1 - \alpha_2), \tag{3.7}$$

where g' is the "reduced gravity" defined by $g' = g(\Delta\rho/\rho)$.

b. Boundary conditions. According to the basin geometry and the assumption of uniform flow at the mouth, the boundary conditions are:

$$\Psi = 0 \qquad ; y = b + x \tan \alpha_1 \qquad ; \quad 0 \leqslant x < \infty \tag{3.8a}$$

$$\Psi = -U_o H_o (y-b) \; ; -b \leqslant y \leqslant b \qquad ; \quad x = 0 \tag{3.8b}$$

$$\Psi = 2U_o H_o b \qquad ; y = -(b + x \tan \alpha_1) \qquad ; \quad 0 \leqslant x < \infty. \tag{3.8c}$$

For reasons that will be addressed shortly, we also require that all streamlines originate from the mouth and that there are no other streamlines in the basin. This condition can be written as:

$$0 \leqslant \Psi(0,y) \leqslant 2U_o H_o b \text{ for all } \Psi\,, \tag{3.8d}$$

which states that *all* Ψ must possess a value between zero and $2U_o H_o b$ for $x = 0$ so that all streamlines cross the y axis. Note that although this condition may appear to be similar to (3.8b), the two conditions are not identical. While the former (3.8b) gives the distribution of Ψ across the mouth, the latter (3.8d) states that there cannot be any streamline which does not originate at the mouth. Condition (3.8d) is, in principle, equivalent to the "radiation condition" which allows the fluid to flow out in the basin but does not allow the fluid to flow in. It is arrived at by the following reasoning.

One intuitively recognizes that a reverse flow extending from infinity to the mouth cannot exist because the outflow is defined as a source and not as a sink. Consequently, if reverse flow exists in the basin then it must have originated at infinity and must also return to infinity without reaching the mouth. Such a reverse flow, which does not correspond to parcels which originated upstream, must be separated from the main outflow by a free dividing streamline. Due to the absence of friction and time dependent motions, there is no mechanism by which lateral momentum can be transferred across such a free dividing streamline. Since there are no sources of momentum in the basin other than the outflow itself, it follows that even the smallest amount of *vertical* friction will bring those regions into which the outflow does not penetrate, quickly to rest. One concludes, therefore, that such regions must be motionless everywhere and cannot contain any flow positive or negative. This gives the condition that reverse flow from infinity is impossible so that there cannot be any streamlines which do not originate at the mouth. Note that while this condition (3.8d) excludes the possibility of reverse flow extending from infinity, it does not exclude the possibility of a reversal of the outflow itself.

As we shall see, conditions (3.8a-d) are sufficient to determine a unique solution. It is important to note, however, that conditions (3.8a) and (3.8c) are valid as long as the flow occupies the whole basin and touches both walls. As we shall see later, the flow cannot occupy the entire basin's width beyond a "critical" distance from

the mouth. In such regions (3.8a-d) are no longer relevant and should be replaced by new conditions.

c. Dimensional and perturbation analysis. We shall first determine the velocity and length scales appropriate to the problem. Since the flow in the basin is a discharge-driven flow the velocity scale is: Ψ_o/lH_o, where Ψ_o is the fresh water discharge ($2U_obH_o$) and l is the, as yet, unknown length scale. This velocity scale is also equal to $l/(\beta l)^{-1}$ because $(\beta l)^{-1}$ is the appropriate time scale for the problem. Hence, the length scale l is found to be:

$$l = (\Psi_o/\beta H_o)^{1/3}. \tag{3.9}$$

For the Amazon outflow (3.9) gives $l \sim 80$ km, which is considerably larger than the mouth's width ($\sim$ 10km). Note that the equatorial deformation radius $[(g'(H_o)^{\frac{1}{2}}/\beta^{\frac{1}{2}}]$ is not a relevant length scale to our problem because the typical speed in the basin is externally imposed and is not related to the speed of an internal gravity wave.

The small ratio between the mouth's width and the length scale in the open ocean suggests that geometrically the feeding channel can be approximately represented by a point source. Although it is clear that such a geometrical approximation can be made, it is necessary to use a detailed perturbation scheme in order to obtain the proper governing equations for a point source. For this purpose, the following nondimensional scaled variables are defined:

$$\begin{aligned} &x^* = x/l \quad ; \quad y^* = y/l \quad ; \quad \Psi^* = \Psi/2U_oH_ob \\ &h^* = h/H_o \quad ; \quad \epsilon = (b/l) << 1 \quad ; \quad u^* = u/U_o(b/l) \\ &v^* = v/U_o(b/l) \; ; \quad \nabla = l\nabla_H \quad ; \quad F = U_o/(g'H_o)^{\frac{1}{2}}, \end{aligned} \tag{3.10}$$

where F denotes the Froude number. In terms of these nondimensional variables the governing equations (3.6) and (3.7) are:

$$\nabla \cdot \left(\frac{\nabla\Psi^*}{h^*}\right) + x^* \cos(\alpha_1-\alpha_2) + y^* \sin(\alpha_1-\alpha_2) - \epsilon h^*(1-2\Psi^*)\sin(\alpha_1-\alpha_2) = 0 \tag{3.11}$$

$$(h^*-1) - \frac{F^2}{2}\left[\, 1-4\epsilon^2\,(\nabla\Psi^*/h^*)^2 + 2\epsilon^3\,(1-2\Psi^*)^2 \sin(\alpha_1-\alpha_2) \,\right] = 0. \tag{3.12}$$

The nondimensional boundary conditions and the "radiation condition" are found from (3.10) and (3.8) to be:

$$\Psi^* = 0 \quad ; \quad y^* = (x^* \tan\alpha_1 + \epsilon) \quad ; 0 < x^* < \infty \tag{3.13a}$$

$$\Psi^* = \tfrac{1}{2}\left[1 - \frac{y^*}{\epsilon}\right]; \quad -\epsilon \leqslant y^* \leqslant +\epsilon \quad ; x^* = 0 \tag{3.13b}$$

$$\Psi^* = 1 \quad ; \quad y^* = -(x^* \tan\alpha_1 + \epsilon) \quad ; 0 \leqslant x^* < \infty \tag{3.13c}$$

$$0 \leqslant \Psi^*(0,y^*) \leqslant 1 \text{ for } \textit{all } \Psi^*. \tag{3.13d}$$

Note that the lefthand side of (3.13b) is well-behaved even if $\epsilon \to 0$ because y^* is always smaller or equal to ϵ. As previously, (3.13d) indicates that all Ψ^* intersects the y^* axis when $x^* = 0$ ensuring that all streamlines originate from the mouth so that there is no reverse flow extending from infinity.

It is further assumed that the two unknowns Ψ^* and h^* can be expanded in power series:

$$\Psi^*(x^*,y^*,\alpha_1,\alpha_2,F,\epsilon) = \Psi^{(o)}(x^*,y^*,\alpha_1,\alpha_2,F) + \epsilon\Psi^{(1)}(x^*,y^*,\alpha_1,\alpha_2,F) + \ldots \tag{3.14a}$$

$$h^*(x^*,y^*,\alpha_1,\alpha_2,F,\epsilon) = h^{(o)}(x^*,y^*,\alpha_1,\alpha_2,F) + \epsilon h^{(1)}(x^*,y^*,\alpha_1,\alpha_2,F) + \ldots, \tag{3.14b}$$

where the Froude number is not necessarily small: $F \lesssim 1$. By substitution of (3.14) into (3.11) and (3.12), and collecting terms of order unity the following zeroth-order equations are obtained:

$$\nabla \cdot (\nabla\Psi^{(o)}/h^{(o)}) = -[x^* \cos(\alpha_1 - \alpha_2) + y^* \sin(\alpha_1 - \alpha_2)] \tag{3.15}$$

$$h^{(o)} = 1 + F^2/2. \tag{3.16}$$

Similarly, the zeroth-order boundary conditions and the radiation conditions are found from (3.14) and (3.13) to be:

$$\Psi^{(o)} = 0 \quad ; \quad y^* = x^* \tan\alpha_1 \quad ; \quad 0 \leqslant x^* < \infty \tag{3.17a}$$

$$\Psi^{(o)} = 1 \quad ; \quad y^* = -x^* \tan\alpha_1 \quad ; \quad 0 \leqslant x^* < \infty \tag{3.17b}$$

$$0 \leqslant \operatorname{Lim}_{y^* \to 0} \Psi^{(o)}(0,y^*) \leqslant 1 \text{ for all } \Psi^{(o)} \; . \tag{3.17c}$$

Note that (3.17) does not include any condition equivalent to (3.13b) since the channel width degenerates to a point when $\epsilon \to 0$. In a similar fashion to (3.13d) and (3.8d), condition (3.17c) states that all transport functions ($\Psi^{(o)}$) must posses a value (between zero and unity) as $x^* \to 0$ and $y^* \to 0$; this ensures that all streamlines originate from the mouth.

Eqs. (3.15)-(3.17) show that the perturbation scheme removed the nonlinearity from the problem and by giving an explicit expression for $h^{(o)}$ [(3.16)], it reduced the number of unknowns from two (Ψ^* and h^*) to one [$\Psi^{(o)}$].

Since $h^{(o)}$ is now known, it is convenient to write (3.15) in the form:

$$\nabla^2\Psi^{(o)} = -[x^* \cos(\alpha_1 - \alpha_2) + y^* \sin(\alpha_1 - \alpha_2)]\,(1 + F^2/2), \tag{3.18}$$

which states that to zeroth-order the relative vorticity [$\xi = \partial v^{(o)}/\partial x^* - \partial u^{(o)}/\partial y^* = \nabla^2\Psi^{(o)}/(1 + F^2/2)$] decreases linearly with x^* and y^*. That is, the farther a parcel of fluid advances, the larger will be its negative relative vorticity which is generated to compensate for the gain in planetary vorticity.

4. Zeroth-order solution

The solution of the zeroth-order equation (3.18) consists of a homogeneous part ($\Psi_H{}^{(o)}$) which satisfies the Laplace equation, and a particular solution ($\Psi_P{}^{(o)}$) whose Laplacian gives the righthand side of (3.18). The boundary conditions for the homogeneous solution are identical to (3.17). The particular solution should vanish on both the southern and northern coasts and together with ($\Psi_H{}^{(o)}$) should satisfy the condition (3.17c) everywhere if the solution is to be valid in the whole field. Under such conditions the sum of the homogeneous and the particular solution will satisfy the complete boundary conditions (3.17).

The homogeneous solution $\Psi_H{}^{(o)}$ satisfying $\nabla^2\Psi_H{}^{(o)} = 0$ and (3.17a-c) is found by elementary methods, such as conformal mapping, to be:

$$\Psi_H{}^{(o)} = [1 - \frac{1}{\alpha_1}\tan^{-1}(y^*/x^*)]/2, \tag{4.1}$$

which describes straight streamlines corresponding to a purely radial motion.

It is important to note that this homogeneous solution corresponds to the total solution on a nonrotating plane ($\beta = 0$). This cannot be easily verified from (3.18) because the scaling that we have used involves ($1/\beta$). However, it can be verified from (3.6) and (3.7) by substituting $\beta = 0$ and neglecting terms which involve the square of the velocity in the field.

The particular solution is found as follows. We take the general form of the particular solution to be a third order polynomial because the Laplacian of such a polynomial gives a linear function of x^* and y^* as required by (3.18). Hence we take:

$$\Psi_P{}^{(o)} = \sum_{k=0}^{3}\sum_{n=0}^{k} A_{nk}\, x^n y^{k-n}. \tag{4.2}$$

The coefficients A_{nk} are found by inserting (4.2) into (3.18), and by considering the two boundary conditions: $\Psi_P{}^{(o)} = 0$ at $y^* = \pm x^* \tan\alpha_1$. Such considerations give:

$$\left.\begin{aligned} &A_{00} = A_{01} = A_{11} = A_{02} = A_{12} = A_{22} = 0\\ &A_{03} = (1 + F^2/2)\sin(\alpha_1 - \alpha_2)/2(\tan^2\alpha_1 - 3)\\ &A_{13} = (1 + F^2/2)\cos(\alpha_1 - \alpha_2)/2(3\tan^2\alpha_1 - 1)\\ &A_{23} = -(1 + F^2/2)\tan^2\alpha_1 \sin(\alpha_1 - \alpha_2)/2(\tan^2\alpha_1 - 3)\\ &A_{33} = -(1 + F^2/2)\tan^2\alpha_1 \cos(\alpha_1 - \alpha_2)/2(3\tan^2\alpha_1 - 1) \end{aligned}\right\} \tag{4.3}$$

From (4.1), (4.2) and (4.3) one finds that the total solution $[\Psi_H{}^{(o)} + \Psi_P{}^{(o)}]$ is:

$$\Psi^{(o)} = \tfrac{1}{2}\left[1 - \frac{\tan^{-1}(y^*/x^*)}{\alpha_1}\right] + [(y^*)^2 - (x^*)^2\tan^2\alpha_1]\left[\frac{y^*\sin(\alpha_1-\alpha_2)}{(\tan^2\alpha_1 - 3)}\right.$$
$$\left. + \frac{x^*\cos(\alpha_1-\alpha_2)}{(3\tan^2\alpha_1 - 1)}\right](1 + F^2/_2)/2\ . \tag{4.4}$$

This solution satisfies the governing equation (3.18) and the boundary conditions along the walls (3.17a and b) for all x^* but, as we shall see, it satisfies the radiation condition (3.17c) only up to a certain distance from the mouth. Beyond this point (4.4) is not valid, and to satisfy the radiation condition and (3.17a-b) it is necessary to allow for separation or blocking to occur. We shall show that this results from the fact that the increase in relative vorticity (which a parcel experiences as it advances into the wedge) imposes a limit on the possible growth of the outflow width. This forces a separation from the walls or a formation of stagnant domains, in regions where the outflow width cannot grow as fast as the width of the wedge does.

The solution (4.4) possesses two singularities; one occurs when $\alpha_1 = \pi/3$ (corresponding to $\tan^2\alpha_1 = 3$) and the other when $\alpha_1 = \pi/6$ ($\tan^2\alpha_1 = 1/3$). It will be shown later that these singularities are a direct result of our perturbation analysis which breaks down when $\alpha_1 \to \pi/3$ or $\alpha_1 \to \pi/6$.

To analyze the solution (4.4) and to investigate the nature of these singularities we shall consider first the relatively simple cases of outflows spreading in eastward basins (i.e., basins whose axes of symmetry coincide with the equator and their outlets are directed toward the east). These simple cases will shed light on the processes involved. The next steps will be to analyze outflows spreading in northward basins and outflows whose basins' outlets are directed toward the northeast as is the case with the Amazon's basin.

5. Eastward basins

For eastward basins $[(\alpha_1 - \alpha_2) = \pi/2]$ (4.4) reduces to:

$$\Psi^{(o)} = \tfrac{1}{2}\left[\, 1 - \frac{1}{\alpha_1}\tan^{-1}(y^*/x^*) \,\right] + \left[\, (y^*)^2 - (x^*)^2\tan^2\alpha_1 \,\right] \times y^*\,(1 + F^2/2)/2\tan^2\alpha - 3), \tag{5.1}$$

which does not involve the term $(3\tan^2\alpha_1 - 1)^{-1}$. We shall first discuss the regions in the vicinity of the mouth where (5.1) satisfies both the conditions at the walls and the radiation condition. In these regions there is no separation or blocking and (5.1) is a valid solution to the problem.

As pointed out earlier with regard to (4.1), the first term on the righthand side of (5.1) (the homogeneous solution) corresponds to the solution in the absence of rotation ($\beta = 0$) and the second is the contribution of the β effect. The sign of the latter term depends on whether $\alpha_1 > \pi/3$ or $\alpha_1 < \pi/3$, which shows that the direction of the β effect crucially depends on the angle between the coastlines. Typical solutions corresponding to this behavior are shown in Figures 3a and 3b. These figures indicate that when $\alpha_1 < \pi/3$ the flow tends to concentrate near the walls, whereas when $\alpha_1 > \pi/3$ the flow is deflected away from the walls.

We shall now show that this dependence of the direction of deflection on α_1

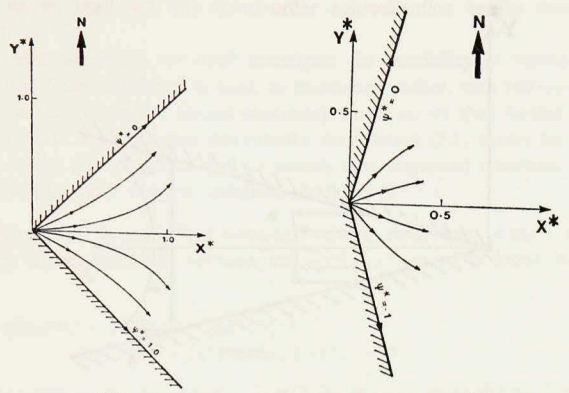

(a) (b)

Figure 3a. Equal transport lines of an outflow spreading in a narrow ($\alpha_1 < \pi/3$) eastward basin ($\alpha_1 = 45°$; $\alpha_2 = -45°$; $F = 0.15$). The flow migrates from the center toward the walls because the changes of planetary vorticity, that a parcel experiences due to the spreading, are offset mainly by horizontal shear (see text). Farther downstream, the tendency of the flow to deflect toward the walls becomes so large that a motionless region is formed in the center of the basin (Fig. 7).

3b. Equal transport lines of an outflow spreading in a wide eastward basin ($\alpha_1 = 75° > \pi/3$; $\alpha_2 = -15°$; $F = 0.15$). In contrast to a narrow outflow (Fig. 3a), the flow migrates toward the center because the changes of planetary vorticity that a parcel experiences are offset mainly by curvature vorticity (see text). Note that the tendency of the flow to deflect away from the walls increases with x^*. Farther downstream the tendency of the flow to deflect away from the walls becomes so large that the fluid cannot cling to the coasts (Fig. 5).

results from the fact that in a narrow wedge ($\alpha_1 < \pi/3$) the changes in planetary vorticity that a parcel experiences due to the spreading of the flow, are compensated mainly by shear ($\partial u^{(o)}/\partial y^*$), whereas in a wide wedge ($\alpha_1 > \pi/3$) the changes are compensated mainly by curvature vorticity ($\partial v^{(o)}/\partial x^*$). To show this we shall examine the velocity field.

The horizontal velocity component in the x direction is found from (5.1) to be:

$$u^{(o)} = x^*/2\alpha_1\,(1 + F^2/2)\,[(x^*)^2 + (y^*)^2] + [(x^*)^2 \tan^2\alpha_1 - 3(y^*)^2]/2\,(\tan^2\alpha_1 - 3), \tag{5.2}$$

which for a very narrow wedge ($\alpha_1 << \pi$) reduces to:

$$u^{(o)} = [2\alpha_1 x^*\,(1 + F^2/_2)]^{-1} - [(x^*)^2\alpha_1{}^2 - 3(y^*)^2]/6. \tag{5.3}$$

This velocity distribution is shown schematically in Figure 4 which indicates that

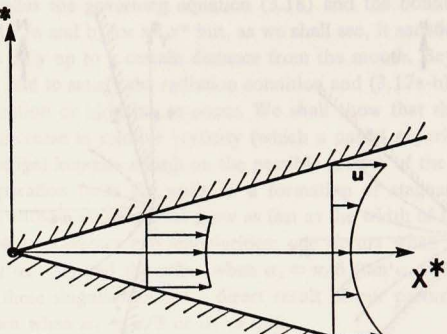

Figure 4. Schematic diagram of the velocity distribution corresponding to an outflow spreading in a very narrow ($\alpha_1 << \pi$) eastward wedge. Central blocking occurs farther downstream (see text).

for a given x^*, $u^{(o)}$ increases with $|y^*|$ and is parabolically distributed. That is, the flow deflects to the left (right) in the northern (southern) hemisphere. In view of this, and the fact that in a very narrow wedge shear dominates (i.e., $\partial u^{(o)}/\partial y^* >> \partial v^{(o)}/\partial x^*$ since $\alpha_1 << \pi$, and $y^* << x^*$), one concludes that a deflection to the left (right) in the northern (southern) hemisphere is caused when changes in planetary vorticity are compensated mainly by shear. It is easy to show [with the aid of (5.1)] that shear dominates the outflow not only in a very narrow wedge but in all wedges whose angles (α_1) are less than $\pi/3$. This indicates that an eastward outflow will migrate toward the coasts for any $\alpha_1 < \pi/3$ [i.e., any outflow with $\alpha_1 < \pi/3$ will behave in a similar fashion to that shown by our numerical example (Fig. 3a)].

It is clear, on the other hand, that if changes in planetary vorticity are compensated mainly by curvature vorticity (i.e., $\partial v^{(o)}/\partial x^* > \partial u^{(o)}/\partial y^*$) then a parcel which is displaced northward (in the northern hemisphere) and has an anticyclonic vorticity will be deflected to the right (i.e., away from the walls). One can easily show, with the aid of (5.1), that this is the case when $\alpha_1 > \pi/3$. This demonstrates that the dependence of the direction of deflection on α_1 is directly related to the relative importance of shear and curvature vorticity. As α_1 increases from, say, 20° [for which shear dominates (i.e., $\partial u^{(o)}/\partial y^* > \partial v^{(o)}/\partial x^*$)] the curvature vorticity ($\partial v^{(o)}/\partial x^*$) also increases until it overcomes the shear (at $\alpha_1 > \pi/3$) and causes a deflection in the opposite direction. Note that in view of this, it is expected that at $\alpha_1 = \pi/3$ there will not be any deflection; this cannot, however, be demonstrated

because, as we shall see, the zeroth-order approximation breaks down when $\alpha_1 \to \pi/3$.

In the next subsection we shall investigate the possibility of separation and blocking (the term "blocking" is used, as mentioned earlier, with reference to regions into which the outflow cannot penetrate). To do so we shall further examine the velocity field to see whether downstream the solution (5.1) allows for negative velocities which do not correspond to parcels that originated upstream, and are therefore incompatible with the radiation condition (3.17c).

a. Separation from the walls. The horizontal velocity component in the x direction, along both the southern and northern wall [$|y^*| = x^* \tan \alpha_1$] is found from (5.2) to be:

$$u^{(o)} = [2\alpha_1 x^*(1 + F^2/2)\,(1 + \tan^2\alpha_1)]^{-1} - (x^*)^2 \tan^2\alpha_1/(\tan^2\alpha_1 - 3). \tag{5.4}$$

This relationship shows that when $\alpha_1 > \pi/3$ the velocity along the walls decreases with x^* and vanishes at:

$$x^*_{vw} = [(\tan^2\alpha_1 - 3)/2\alpha_1\,(1 + F^2/2)\,(1 + \tan^2\alpha_1)\,\tan^2\alpha_1]^{1/3}, \tag{5.5}$$

where the subscript "vw" denotes that the variable in question is associated with vanishing velocity at the wall. Note that, at the walls the total velocity vanishes when $u^{(o)} = 0$ since $u^{(o)} = |v^{(o)}|/\tan\alpha_1$, and that elsewhere in the basin $u^{(o)} > 0$ for all y^* and $x^* \leqslant x^*_{vw}$.

Along the walls the flow cannot advance farther than x^*_{vw} because for $x^* > x^*_{vw}$ the velocity becomes negative [according to (5.4)] corresponding to streamlines that do not originate upstream and are, therefore, impossible. It follows that at $x^* = x^*_{vw}$ the flow must separate from the walls (i.e., for the radiation condition to be satisfied we must allow the flow to detach from the walls). Beyond the separation points the flow is bounded by two free streamlines one at each edge. A typical solution which includes the separation points is shown in Figure 5. We see that the separation is consistent with the general direction of deflection discussed earlier. We saw earlier that the farther a parcel of fluid advances the larger is its tendency to deflect away from walls (Fig. 3b). Consequently, a parcel advancing along the coast reaches a point [(C) or (D)] where it can no longer cling to the wall.

The solution (5.1) is valid for all $x^* \leqslant x^*_{vw}$ (including the separation points) but is not valid for $x^* > x^*_{vw}$; in such regions the boundary conditions that we used for the walls (3.17a, b) are no longer relevant and should be replaced by new conditions which involve the unknown location of the free bounding streamlines. The solution for the separated outflow (i.e., for $x^* > x^*_{vw}$) is beyond the scope of this study, but we shall give the new boundary conditions in order to show that the problem is well defined in such regions. The new boundary conditions are:

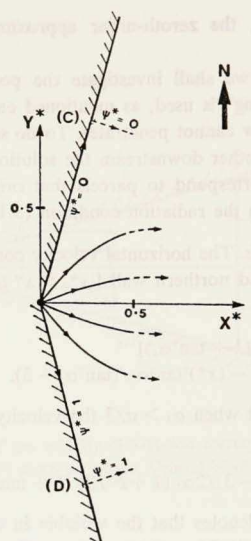

Figure 5. Equal transport lines of an outflow spreading in a wide eastward basin ($\alpha_1 = 75° > \pi/3$; $\alpha_2 = -15°$; $F = 0.15$). The outflow separates from the walls at (C) and (D). To illustrate the separation process and the formation of blocked regions (to the north and south of the separating streamlines), the solution (5.1) was extrapolated for a short distance beyond the separation points (dashed lines).

$$\Psi^{(o)} = 0; \qquad y^* = \gamma_1(x^*) \qquad ; x^*_{vw} \leqslant x^* < \infty \tag{5.6a}$$

$$(\nabla\Psi^{(o)}/h^{(o)})^2 = 0; \qquad y^* = \gamma_1(x^*) \qquad ; x^*_{vw} \leqslant x^* < \infty \tag{5.6b}$$

$$\Psi^{(o)} = \Psi^{(o)}(y^*); \quad -x^*_{vw}\tan\alpha_1 \leqslant y^* \leqslant x^*_{vw}\tan\alpha_1; x^* = x^*_{vw} \tag{5.6c}$$

$$\Psi^{(o)} = 1; \qquad y^* = \gamma_2(x^*) \qquad ; x^*_{vw} \leqslant x^* < \infty \tag{5.6d}$$

$$(\nabla\Psi^{(o)}/h^{(o)})^2 = 0; \qquad y^* = \gamma_2(x^*) \qquad ; x^*_{vw} \leqslant x^* < \infty \tag{5.6e}$$

$$0 \leqslant \Psi^{(o)}(x^*_{vw}, y^*) \leqslant 1 \text{ for all } \Psi^{(o)} \tag{5.6f}$$

Conditions (5.6a) and (5.6d) state that the location and shape of the free bounding streamlines [$\gamma_1(x^*)$; $\gamma_2(x^*)$] are not known in advance and must be determined as part of the flow. Conditions (5.6b) and (5.6e) state that the velocity is zero along the free bounding streamline; this condition compensates for the fact that the location and shape of the free bounding streamlines are not given *a priori*. It results from an application of the Bernoulli principle along the free bounding streamlines and indicates that the free surface height does not vary along the bounding streamlines. This ensures that the "blocked" regions are motionless everywhere. Similar

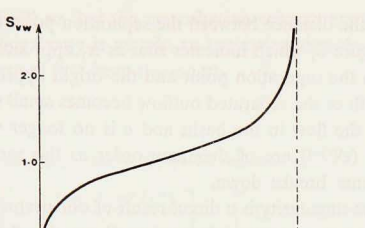

Figure 6. The dependence of the distance between the mouth and the separation points ($s_{vw} = x^*_{vw} \cos \alpha_1$) on the opening angle ($2\alpha_1$) of a wide eastward basin ($\alpha_1 > \pi/3$; $F = 0.15$).

free streamline conditions are discussed by Stern (1975), Batchelor (1967), Ingersoll (1969) and Garabedian (1964). For solutions which involve actual computation of a free streamline location and shape see, for example, Anderson and Moore (1979), and Nof (1980).

Condition (5.6c) reflects the known distribution $\Psi^{(0)}$ along y^* at $x^* = x^*_{vw}$ [obtained from the known solution (5.1)], and condition (5.6f) is the radiation condition [equivalent to (3.13d)]. As mentioned above, we shall not seek solutions for the separated outflows; we have presented the modified boundary conditions only to show that they are sufficient to determine a solution which will be valid for $x^* > x^*_{vw}$.

We shall now discuss the nature of the singularity occuring when $\alpha_1 \to \pi/3$ (i.e., $\tan^2\alpha_1 \to 3$). The singularity corresponding to an angle approaching $\pi/3$ from above (i.e., $\alpha_1 \to \pi/3$; $\alpha_1 > \pi/3$) will be addressed first; the complementary singularity, corresponding to an angle approaching $\pi/3$ from below (i.e., $\alpha_1 \to \pi/3$; $\alpha_1 < \pi/3$), will be discussed in the next subsection.

The nature of the singularity can be understood by examining the first-order equations and the sensitivity of the distance between the separation point and the mouth ($s_{vw} = x^*_{vw}/\cos\alpha_1$) to α_1. The first-order equations are found [by substituting (3.14) into (3.11-3.12), collecting terms of order ϵ, and considering (3.16)] to be:

$$h^{(1)} = 0,$$

and

$$\nabla^2\Psi^{(1)} = (1 + F^2/_2)^2(1 - 2\Psi^{(0)})\sin(\alpha_1 - \alpha_2).$$

These equations show that the first correction to the depth is zero and that the correction to the transport function ($\epsilon\Psi^{(1)}$) is of $0(\epsilon)$ since $\Psi^{(1)} \sim 0(\Psi^{(0)})$. In view of this, it is expected that the perturbation scheme will not be singular as long as ϵ is small compared to unity.

The sensitivity of the distance between the separation point and the origin (s^*_{vc}) to α_1 is shown in Figure 6, which indicates that as α_1 approaches $\pi/3$ from above, the distance between the separation point and the origin approaches zero. That is, as $\alpha_1 \to \pi/3$ the width of the separated outflow becomes small so that l is no longer the proper scale for the flow in the basin and ϵ is no longer small. Consequently, the first-order terms ($\epsilon\Psi^{(1)}$) are of the same order as the zeroth-order terms and the pertubation scheme breaks down.

This shows that the singularity is a direct result of our perturbation scheme which is incapable of giving the correct information about the flow in the immediate vicinity of the mouth where the length scale is of $0(b)$ rather than of $0(l)$. In other words, the singularity is merely an indication that the separation point is located within a distance of $0(b)$ from the mouth.

To obtain the proper solution for $\alpha_1 \to \pi/3$ it is necessary to rescale the variables and take the length scale in the basin (l) to be equal to b. That is, ϵ must be taken to be unity and the full nonlinear equations [(3.11)-(3.12) with $\epsilon = 1$] should be solved. This is beyond the scope of the present study.

b. Central blocking. In the previous subsection it has been demonstrated that for $\alpha_1 > \pi/3$ the outflow separates from both walls at a "critical" distance from the mouth. We shall now demonstrate that when $\alpha_1 < \pi/3$ the outflow splits into two branches and forms a blocked region in the center of the basin.

Examination of (5.2) indicates that when $\alpha_1 < \pi/3$, the velocity along the basin's axis ($y^* = 0$) decreases with x^* and vanishes at:

$$x^*_{vc} = [(3 - \tan^2\alpha_1)/\alpha_1\,(1 + F^2/2)\tan^2\alpha_1]^{1/3}\,, \tag{5.7}$$

where the subscript "vc" indicates that the variable in question is associated with vanishing velocity at the center of the basin. The flow cannot advance farther along the axis, because a reverse velocity will be generated and such a reverse velocity does not correspond to parcels which have originated upstream. Hence, beyond the stagnation point the outflow must consist of two symmetrical branches each of which is bounded by a solid wall and a free streamline as indicated in Figure 7 which shows a typical outflow spreading in a narrow basin ($\alpha_1 < \pi/3$). Note that the radiation condition cannot be satisfied unless we allow the branching to occur. The solution (5.1) is valid for all $x^* \leqslant x^*_{vc}$ but must be modified for $x^* > x^*_{vc}$. In a similar fashion to the wide basin case, we shall not seek solutions for this region where the flow does not occupy the entire basin's width. However, it is easy to show that, as previously, the problem is well defined in such regions.

Before concluding our present discussion it is appropriate to comment on the relationship between the singularity at $\alpha_1 \to \pi/3$ to the mechanism of branching discussed above. Eq. (5.7) shows that as α_1 approaches $\pi/3$ from below (i.e., $\alpha_1 < \pi/3$) the stagnation point ($x^* = x^*_{vc}$) approaches the origin. Under such conditions, the width of the branched outflow is of the same order as the width of the mouth

(i.e., ϵ is no longer small) so that the perturbation scheme breaks down. As in the wide basin case, the singularity is merely an indication that the stagnation point is located within a distance of $0(\epsilon)$ from the mouth.

6 Northward basins

For northward basins $[(\alpha_1 - \alpha_2) = 0]$ (4.4) reduces to:

$$\Psi^{(0)} = \tfrac{1}{2}\left[1 - \frac{\tan^{-1}(y^*/x^*)}{\alpha_1}\right] + \left[(y^*)^2 - (x^*)^2\tan^2\alpha_1\right] \times \frac{x^*(1 + F^2/2)}{2(3\tan^2\alpha_1 - 1)}, \tag{6.1}$$

which does not involve the term $(\tan^2\alpha_1 - 3)^{-1}$. Typical solutions for $\alpha_1 < \pi/6$ (corresponding to $\tan^2\alpha_1 < 1/3$) and for $\alpha_1 > \pi/6$ are shown in Figures 8a and b. We see that when $\alpha_1 < \pi/6$ the flow migrates toward the west (left) whereas when $\alpha_1 > \pi/6$ the flow migrates toward the east (right). In a similar fashion to the eastward outflow case, this behavior results from the fact that when $\alpha_1 < \pi/6$, changes in planetary vorticity, that a parcel experience due to the spreading, are offset mainly by shear (i.e., $\partial u^{(0)}/\partial y^* > \partial v^{(0)}/\partial x^*$), whereas when $\alpha_1 > \pi/6$ the changes are compensated mainly by curvature vorticity (i.e., $\partial v^{(0)}/\partial x^* > \partial u^{(0)}/\partial y^*$).

Examination of the velocity field indicates that central blocking is impossible for all α_1; however, the flow separates from either the eastern or the western wall depending on the magnitude of α_1 (Fig. 8). The locations at which the velocity vanishes (i.e., the separation points) are:

$$x^*_{sl} = [(3\tan^2\alpha_1 - 1)/2\alpha_1\,(1 + F^2/2)\tan\alpha_1\,(1 + \tan^2\alpha_1)]^{1/3};\ \alpha_1 > \pi/6 \tag{6.2}$$

and

$$x^*_{sr} = [(1 - 3\tan^2\alpha_1)/2\alpha_1\,(1 + F^2/2)\tan\alpha_1\,(1 + \tan^2\alpha_1)]^{1/3};\ \alpha_1 > \pi/6 \tag{6.3}$$

where the subscripts "*sl*" and "*sr*" denote that the variable in question is associated with a separation from the left and right walls respectively.

The singularity at $\alpha_1 = \pi/6$ represents, as previously, the condition at which the separation point is located within a distance of $0(\epsilon)$ from the origin. When α_1 approaches $\pi/6$ from above (i.e., $\alpha_1 > \pi/6$) the separation from the western wall approaches the origin, whereas when α_1 approaches $\pi/6$ from below (i.e., $\alpha_1 < \pi/6$) the separation from the eastern wall approaches the origin. Under both conditions the perturbation scheme breaks down and the solution (6.1) is not valid.

7. The Amazon outflow

The Amazon's basin corresponds to a wide wedge ($\alpha_1 > \pi/3$) whose axis of symmetry is directed approximately toward the NE (Fig. 1). It therefore corresponds

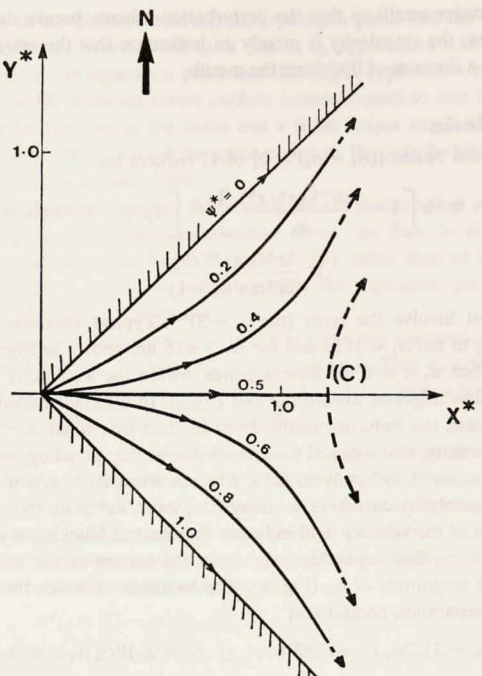

Figure 7. Equal transport lines of an outflow spreading in a narrow ($\alpha_1 < \pi/3$) eastward basin ($\alpha_1 = 45°$; $\alpha_2 = -45°$; $F = 0.15$). The stagnation point (C) represents the edge of the blocked region. To illustrate the central blocking effect, the solution was extrapolated for a short distance beyond the stagnation point (dashed lines).

to a combination of a wide eastward and northward outflow. For such a system one finds from (4.4) that there is no central or off axis blocking within a distance of 0(1) from the origin. However, within this distance, there is a separation from both the left and right walls. The locations of the separation points [as determined from (4.9)] are:

$$x^*_{sl} = \Big[2\alpha_1 (1 + F^2/2)\tan\alpha_1 (1 + \tan^2\alpha_1) [\cos(\alpha_1 - \alpha_2)/(3\tan^2\alpha_1 - 1) - \sin(\alpha_1 - \alpha_2)\tan\alpha_1/(3 - \tan^2\alpha_1)] \Big]^{-1/3} \tag{7.1}$$

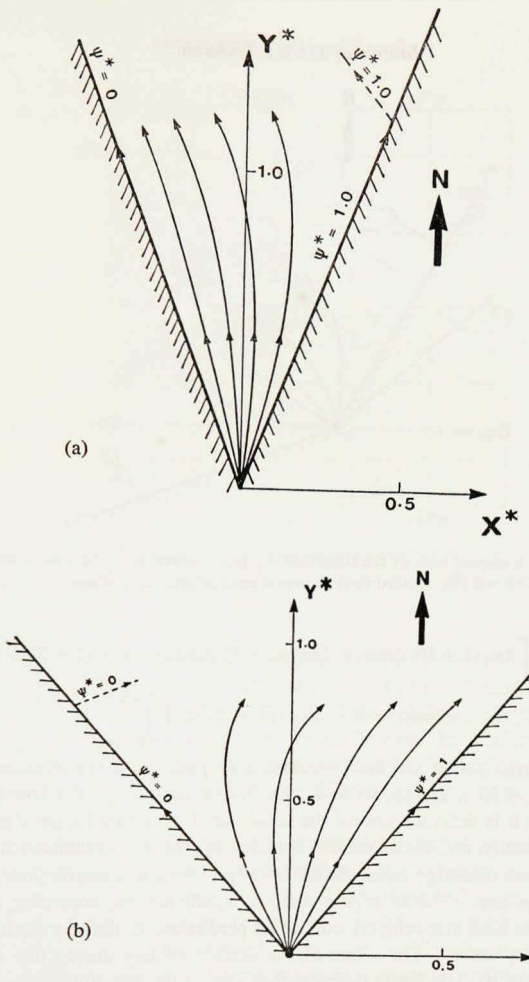

Figure 8a. Equal transport lines of an outflow spreading in a narrow ($\alpha_1 < \pi/6$) northward basin ($\alpha_1 = \alpha_2 = 20°$; $F = 0.15$). In a similar fashion to the narrow eastward outflow (Figs. 3a and 7), the flow is deflected toward the left wall because changes in planetary vorticity are offset mainly by horizontal shear. For clarity the solution (6.1) was extrapolated for a short distance beyond the separation point (dashed line).

8b. The same as (8a) but for a wide ($\alpha_1 > \pi/6$) northward basin ($\alpha_1 = \alpha_2 = 40°$; $F = 0.15$). The flow migrates toward the wall because the changes in planetary vorticity that a parcel experience due to the spreading are compensated mainly by curvature vorticity.

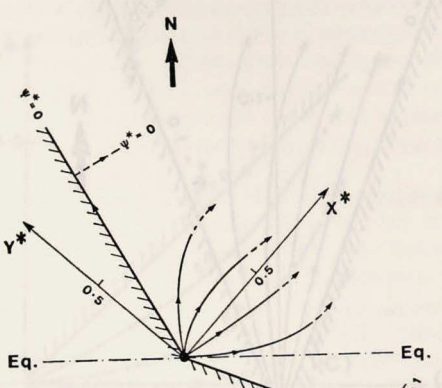

Figure 9. Equal transport lines of the simplified Amazon outflow ($\alpha_1 = 70°$; $\alpha_2 = 30°$) during low discharge ($F \approx 0.10$). Dashed lines represent extrapolated streamlines.

$$x^*_{sr} = \Big[2\alpha_1 (1 + F^2/2)\tan\alpha_1 (\tan^2\alpha_1 + 1) \, [\cos(\alpha_1 - \alpha_2)/(1 - 3\tan^2\alpha_1) - \sin(\alpha_1 - \alpha_2)\tan\alpha_1/(3 - \tan^2\alpha_1)] \Big]^{-1/3}. \tag{7.2}$$

The separation points and the associated flow pattern for the Amazon's basin ($\alpha_1 \approx 70°$; $\alpha_2 \approx 30°$), are shown in Figure 9. We see that as the flow advances into the basin it is deflected toward the center until it can no longer cling to the walls; subsequently, an isolated current bounded by two free streamlines is formed.

The Amazon's discharge varies considerably from season to season [low and high river discharge are ~83,500 m³/sec and ~267,400 m³/sec, according to Gibbs (1970)] and we shall first compare our model predictions to the low discharge season [August-September]. The observed sea surface salinity during this season is shown in Figure 10. This figure indicates that, during the low-discharge period, the actual outflow separates from both the northern and southern coast as predicted by the theoretical model (Fig. 9). However, it is not entirely clear that the actual separation from the coasts (indicated by Fig. 10) results from our proposed mechanism (Fig. 9). It seems that such a separation can also be caused by the Guiana Current (which advects the outflow toward the northwest) and the North Equatorial Counter-current which may carry the outflow toward the east. The salinity structure

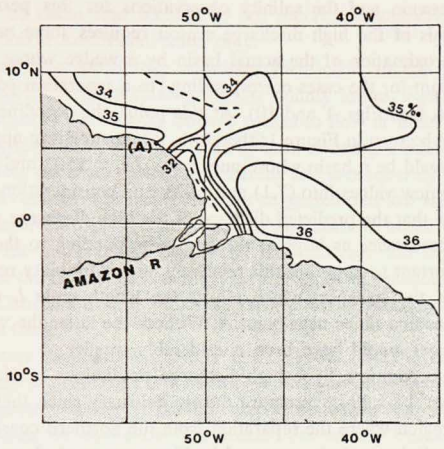

Figure 10. The observed surface salinity in the western tropical Atlantic during September (adapted from Neumann *et al.*, 1975). The axis of the Amazon outflow is represented by the minimum salinity line (– – –).

resulting from these two currents may be similar to that indicated by Figure 10 so that it is impossible to distinguish between the effect of our theoretical separation and that of the local currents system. This question could, perhaps, be partially answered by a detailed, quantitative comparison between the predicted location of the separation points and the actual separation latitudes, but such a comparison is impossible due to our neglect of friction, diffusion and the irregularities of the coastline.

Even though a detailed comparison is impossible, it should be pointed out that for low-discharge the theory predicts separation from both coasts at distances of ~ 150km from the mouth. These are comparable to the actual separation distances (i.e., the distances between the mouth and the points of maximum horizontal density gradient along the coast) indicated by Figure 10. The theoretical separation distances mentioned above have been determined using a modified upper layer transport (Ψ_T) which includes the effect of entrainment, because the main body of the outflow does not consist of water which is entirely fresh but rather of water with an average salinity of 32‰. Following Bowden (1967), the modified transport has been taken to be: $\Psi_T = \Psi_o S_B/(S_B - S_T)$, where S_B is the salinity of the bottom layer (36‰) and S_T is the salinity of the outflow as it leaves the coast (~ 32‰).

We shall now discuss the relationship between the theoretical prediction for the

high discharge season and the salinity observations for this period. A detailed theoretical analysis of the high discharge season requires some new calculations, because our approximation of the actual basin by a wedge whose angle is $2\alpha_1 = 140°$ is not relevant for the cases corresponding to a separation point located farther than point A (see Figs. 1 and 10). At this point, the coastline shape changes drastically as can be seen in Figure 1; therefore, a more realistic approximation for high discharge would be a basin whose angles are $2\alpha_1 = 150°$ and $\alpha_2 = 40°$. Substitution of these new values into (7.1) and (7.2), and consideration of the relevant length scale show that the predicted distance of the high discharge separation from both coasts is about *twice* as large as the one corresponding to the low discharge season. It is important to note that this relatively large variability results from both the variability of the transport which affects the length scale l, and the drastic change of the coastline shape near point A. Without the latter the variability of the separation distances would have been considerably smaller.

It is difficult to compare these high-discharge predictions to Neumann *et al.'s* (1975) analysis of the salinity structure during February since their analysis does not include the region where the separation from the northern coast is expected to take place. The salinity analysis presented by Neumann *et al.* shows, however, that during February there is no separation from the northern coast within a distance of $\sim$ 1200km from the mouth. The southern separation point (i.e., the point of maximum horizontal density gradient along the coast) is located at a distance which is $\sim$150km longer than the one associated with low-discharge. This supports the theoretical prediction of the southern separation variability, but does not give sufficient information about the northern separation variability for the comparison to be entirely satisfactory.

8. Low salinity lenses

In this section we shall discuss the relationship between the model results and the low salinity lenses which have been observed off the South American Coast.

Before addressing the physical mechanisms related to these lenses it is appropriate to comment on the question of their origin because, while it is plausible that the lenses have originated at the Amazon, it is not *a priori* obvious that they do not contain fresh water from other sources. In fact, Neumann (1969) has pointed out that in these regions local precipitation can affect the surface salinity to a noticeable degree. However, Ryther *et al.* (1967) showed a clear association of high silicate concentration and brownish-green water color with the low salinity patches; these facts strongly suggest that the lenses contain Amazonian water. In view of these investigations it is reasonable to suppose that, although the low salinity lenses have probably originated from the Amazon, they may be modified by local precipitation as well as run-off from adjacent areas. This possible modification of the fresh water

masses will not be taken into account in our theoretical analysis which assumes that the lenses contain Amazonian water only.

Several authors have previously addressed themselves to the processes which could be responsible for the formation of low salinity lenses. Ryther *et al.* (1967) suggested that possibly the Guiana Current ceases to flow at times due to slackening or temporary reversal of the local wind system, allowing a bubble or bubbles of river water to cross the main axis of the Current and subsequently become isolated when the current resumes. Metcalf (1968) has suggested that low salinity lenses may be formed as the result of discontinuities in the current north of the Amazon River and near the origin of the Equatorial Undercurrent. He argues that: "The whole picture [of the Guiana Current] suggests a series of meanders and recurving of parts of the Coastal Current, with successive pools of Amazon outflow moving offshore amongst them."

Both the process suggested by Ryther *et al.* (1967) and the one suggested by Metcalf (1968) are possible, but as we shall see, the present study suggests a mechanism which does not require the coastal currents system to have any special structure. In other words, we shall show that isolated low salinity lenses may be formed without any of the previously proposed mechanisms being active.

The proposed mechanism is related to the profound seasonal variability of the outflow discussed earlier in Section 7. We have seen earlier that because of the large seasonal variability of the separation points, the region into which the outflow penetrates during the high discharge season is considerably different than the one occupied during the low discharge season. Consequently, segments of the outflow are left behind after each high discharge season. Such segments become isolated from the main outflow when the outflow returns to its low discharge position and as such, they are out of balance and, therefore, cannot maintain their initial structure. Whatever their shape is, they must undergo an adjustment toward geostrophic balance, close upon themselves and form lenses because the latter is the only possible balanced steady state.

The approximate shape and structure of an Amazonian lens formed by this process can be easily calculated using an approach similar to that used by Flierl (1979) who examined the dynamics of Gulf Stream rings and determined their approximate structure numerically. The purpose of the analysis presented below is to obtain the general structure of an Amazonian lens and to determine the relationship between the lens diameter and depth which can be qualitatively compared to the observations of Ryther *et al.* (1967). The analysis resembles the numerical analysis of Flierl (1979) except that we deal with a fluid which originated from the equator and has zero potential vorticity. This enables us to obtain an exact analytical solution which includes the full nonlinear terms.

The equation for conservation of momentum in the radial direction and the potential vorticity equation in cylindrical coordinates are (see e.g., Flierl, 1979):

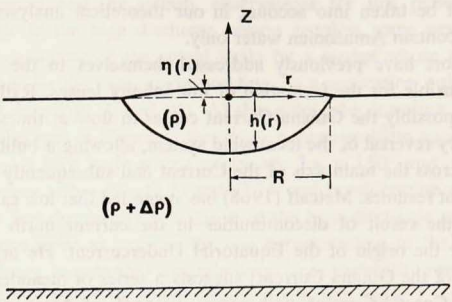

Figure 11. Schematic diagram of an Amazonian lens.

$$\frac{\partial v_r}{\partial t} + v_r \frac{\partial v_r}{\partial r} + \frac{v_\theta}{r} \frac{\partial v_r}{\partial \theta} - \frac{v_\theta^2}{r} - f v_\theta = -g' \frac{\partial h}{\partial r} \tag{8.1}$$

$$\frac{D}{Dt}\left[\left[\partial v_\theta / \partial r + v_\theta / r - (\partial v_r / \partial \theta)/r + f \right] / h \right] = 0 , \tag{8.2}$$

where

$$\frac{D}{Dt} = \frac{\partial}{\partial t} + v_r \frac{\partial}{\partial r} + \frac{v_\theta}{r} \frac{\partial}{\partial \theta} ,$$

and v_r and v_θ are the radial and tangential velocity components respectively. Here, the origin of the coordinates system is taken at the center of the lens (see Fig. 11).

Since the fluid originated from the equator with both relative and planetary vorticity being approximately zero, the potential vorticity must be zero at all times including the ultimate balanced state. Hence, (8.2) gives for the final, balanced steady state:

$$\partial v_\theta / \partial r + v_\theta / r - \frac{1}{r} (\partial v_r / \partial \theta) + f = 0. \tag{8.3}$$

To simplify the analysis, we shall assume that the volume of the isolated fresh water segment which became separated from the mean outflow [$V(m^3)$], is not very large so that its length scale [$0(V/H_0)^{\frac{1}{2}}$] is small compared to its distance from the Amazon's mouth. The validity of this assumption can be determined by examining the 31‰ salinity contour (Fig. 1) which represents the boundary between the lens and the environment [since the average salinity in the core is ~27‰ (determined from Ryther *et al.*, 1967) and the environment salinity is ~35‰]. The shape of this contour suggests that to zeroth-order the assumption is adequate because it corresponds to a lens' radius of ~200km, whereas the distance between the center of the lens and the equator is much larger, about 1000km.

Under such conditions the variation of the Coriolis parameter across the lens is small compared to the Coriolis parameter at the center of the lens (f_o). The analysis is further simplified by assuming that the motion in the lens is purely tangential (i.e., $v_r = 0$ and $\frac{\partial}{\partial\theta} = 0$). For such conditions (8.3) and (8.1) reduce to:

$$\frac{1}{r}\frac{d}{dr}(rv_\theta) = -f_o \tag{8.4}$$

and

$$v_\theta^2/r + f_o v_\theta = g'\frac{dh}{dr}. \tag{8.5}$$

With the condition $v_\theta = 0$ at $r = 0$, (8.4) yields:

$$v_\theta = -f_o r/2, \tag{8.6}$$

which states that the velocity increases linearly with r. Substitution of (8.6) into (8.5) gives:

$$h = \hat{h} - f_o^2 r^2/8g', \tag{8.7}$$

where $\hat{h}$ is the lens depth at the origin. Eq. (8.7) shows that the interface shape is parabolic, and that the interface strikes the surface ($h = 0$) at:

$$R = (8g'\hat{h})^{\frac{1}{2}}/f_o. \tag{8.8}$$

This theoretical prediction can be qualitatively compared to the observed horizontal scale by substituting the observed depth of the 31‰ salinity surface at the center of the lens (~16m, according to Ryther *et al.*, 1967) into (8.8). Such a substitution [together with $g' \approx 0.08$ m/sec^2 and $f_o \approx 0.2 \times 10^{-4}$sec^{-1}] gives an intersection radius of ~150km, a distance comparable to the observed horizontal scale of the 31‰ salinity contour (see Fig. 1). This qualitative agreement supports our conjecture that the lenses result from geostrophic adjustment.

9. Summary

Before listing our conclusions it is perhaps appropriate to stress once more the main limitations of the theoretical analysis. The analysis does not include the effects of friction, diffusion, coastline irregularities and the influence of the Guiana Current which sweeps the actual outflow toward the north. In reality, these processes will, no doubt, influence the flow. Although much work remains to be done before we can adequately understand the behavior of the real system, our present findings give information about isolated processes related to the outflow.

The results of the theory can be summarized as follows:

i) As an equatorial outflow spreads in the basin, the fluid gains relative vorticity in order to compensate for the changes in planetary vorticity. Consequently, the

fluid does not spread uniformly in all directions, but rather is deflected toward or away from the coastlines depending on the basin's geometry. When the angle between the two coastlines forming the basin is small, changes in planetary vorticity which a parcel experiences due to the spreading are offset mainly by generation of horizontal shear; in contrast, when the angle is wide, changes in planetary vorticity are compensated mainly by curvature vorticity. In the latter case the outflow deflects to the right in the northern hemisphere, whereas in the former the outflow deflects to the left.

ii) When the flow reaches a "critical" distance from the mouth the gain in relative vorticity is so large that the flow cannot fill the entire basin's width. Consequently, separation occurs and portions of the basin are blocked in the sense that no parcels which originated upstream can enter them.

iii) The Amazon outflow, whose basin is wide and contains sections of both the southern and the northern hemisphere, is deflected away from the coastlines as it spreads in the basin. At a "critical" distance from the mouth, the gain in curvature vorticity is so large that the fluid can no longer cling to the walls. Subsequently, the flow separates from both walls and penetrates into the ocean interior as an isolated current.

iv) During the high-discharge season separation occurs at distances which are considerably larger than those associated with low discharge. As a result, the location and width of the regions which contain Amazonian water vary considerably from season to season.

Prediction (iii) was compared to the observed surface salinity structure in the western tropical Atlantic and qualitative agreement was noted. Based on conclusion (iv), a mechanism which may be responsible for the formation of low salinity lenses is proposed. It is suggested that these lenses may result from segments of the Amazon outflow which become separated from the main outflow after each high discharge season. Such segments undergo an adjustment toward geostrophic balance to form isolated lenses with anticyclonic vorticity.

Acknowledgments. This study was supported by the National Science Foundation under Grant ATM-77-28126 and by the Office of Naval Research Grant N00014-80-C-0042.

REFERENCES

Anderson, D. L. T. and D. W. Moore. 1979. Cross-equatorial inertial jets with special relevance to very remote forcing of the Somali Current. Deep-Sea Res., *26A*, 1–22.

Batchelor, G. K. 1967. An introduction to fluid dynamics. Cambridge University Press, London, 615 pp.

Bowden, K. F. 1967. Circulation and diffusion, *in* Estuaries. G. H. Lauff, ed., Publ. Amer. Ass. Advanc. Sci., *83*, pp. 15–36.

Davis, L. C., Jr. 1964. The Amazon's rate of flow. Nat. History, *73*, 14–19.

Flierl, G. R. 1979. A simple model for the structure of warm and cold core rings. J. Geophys. Res., *84*, 781–785.

Froelich, P. M., Atwood, D. K. and Giese, G. S. 1978. Influence of Amazon River discharge on surface salinity and dissolved silicate concentration in the Caribbean Sea. Deep-Sea Res., *25*, 735–744.

Garabedian, P. R. 1964. Partial Differential Equations. John Wiley and Sons, N.Y., 672 pp.

Gibbs, R. J. 1970. Circulation in the Amazon River estuary and adjacent Atlantic Ocean. J. Mar. Res., *28*, 113–132.

Gutman, L. M. 1972. Introduction to the Nonlinear Theory of Mesoscale Meteorological Processes. NOAA, U.S. Dept. of Commerce, 224 pp.

Ingersoll, A. R. 1969. Inertial Taylor columns and Jupiter's Great Red Spot. J. Atmos. Sci., *26*, 744–752.

Landis, R. C. 1971. Early BOMEX results of sea surface salinity and Amazon River water. J. Phys. Oceanogr., *1*, 278–281.

Metcalf, W. G. 1968. Shallow currents along the northeastern coast of South America. J. Mar. Res., *26*, 232–243.

Neumann, G. 1969. Seasonal salinity variations in the upper strata of the western tropical Atlantic Ocean — I. Sea surface salinities. Deep-Sea Res., Supplement to vol. 16, 165–177.

Neumann, G., W. H. Beatty III and E. C. Escowitz. 1975. Seasonal changes of oceanographic and marine-climatological conditions in the equatorial Atlantic. City University of New York final report AD-A016290 (available from the National Technical Information Service, U.S. Department of Commerce). 211 pp.

Nof, D. 1978a. On geostrophic adjustment in sea straits and wide estuaries: Theory and laboratory experiments. Part I — one-layer system. J. Phys. Oceanogr., *8*, 690–702.

—— 1978b. On geostrophic adjustment in sea straits and wide estuaries: Theory and laboratory experiments. Part II — two-layer system. J. Phys. Oceanogr., *8*, 861–872.

—— 1980. The influence of varying bathymetry on inertial boundary currents. Tellus, *32*, 284–295.

Paul, J. and W. Lick. 1974. A numerical model for thermal plumes and rivers discharge. Proc. 17th Conf. Great Lakes Res., Int. Assoc. Great Lakes Res., Ann Arbor, 445–455.

Ryther, J. H., D. W. Menzel and N. Corwin. 1967. Influence of the Amazon River outflow on the ecology of the western tropical Atlantic I. Hydrography and Nutrient Chemistry. J. Mar. Res., *25*, 69–83.

Stern, Melvin E. 1975. Ocean circulation physics. Academic Press, New York, 246 pp.

Takano, K. 1954. On the velocity distribution off the mouth of a river. J. Oceanogr. Soc. Japan, *10*, 60–64.

—— 1955. A complementary note on the diffusion of the seaward river flow off the mouth. J. Oceanogr. Soc. Japan, *11*, 147–149.

Received: *23 February, 1980;* revised: *26 August, 1980.*